Application of Transient Eddy Current Analysis to Rotating Machines

Kanayama, Hiroshi
Kyushu University

Sugimoto, Shin-ichiro
The University of Tokyo

Murotani, Kouhei
The University of Tokyo

Terada, Seigo
Kyushu University

他

出版情報：COE Lecture Note. 45, pp.27-43, 2013-02-19. Institute of Mathematics for Industry, Kyushu University
バージョン：
権利関係：

Application of Transient Eddy Current Analysis to Rotating Machines

Hiroshi Kanayama*(Kyushu University), Shin-ichiro Sugimoto (The University of Tokyo),
Kouhei Murotani (The University of Tokyo), Seigo Terada (Kyushu University), Seiya Kuramoto (Kyushu University)

Transient eddy current analysis of rotating machines is considered. NEXST_Magnetic is mainly used in this study. Cases without and with rotor rotation are considered. The accuracy of a simple model is confirmed and a three-phase induction motor is analyzed.

Keywords: Induction motor, Eddy current, Transient analysis, NEXST_Magnetic, ADVENTURE_Magnetic

1. Introduction

Various methods have been considered for three-dimensional time-harmonic eddy current problems and effective numerical calculations have been performed to obtain many results. The A method in which the magnetic vector potential A is the unknown function and the $A-\phi$ method in which both A and the electric scalar potential ϕ are unknown functions have both been demonstrated to be effective for these types of problems. In a previous study, we applied hierarchical domain decomposition to these methods and demonstrated that accurate numerical results for large-scale problems could be obtained by parallel computations [1,2]. However, it is necessary to treat the problem as non-stationary for many real-world phenomena. For time-harmonic three-dimensional eddy current problems, we used the $A-\phi$ method, which exhibits favorable performance from a computation-time perspective. Using the same technique for the space approximation, we now introduce a backward Euler method for time stepping to study transient three-dimensional eddy-current problems [3]. For this purpose, we employed and improved the NEXST_Magnetic software [4]. This software provides a single-processor module for finite-element analysis and allows analysis of nonlinear magnetostatic fields and non-stationary eddy-current analysis for up to tens of millions of degrees of freedom. In this study, we extend this software by adding functionality to consider the *B–H* characteristics of materials [5] and we present computational results obtained using this new functionality. Finally, we discuss a method for addressing the rotation of rotors [6].

2. Eddy Current Problems

2.1 Basic equations and boundary conditions

We consider a polyhedral domain Ω with boundary $\partial\Omega$. The domain Ω consists of two non-overlapping polyhedral subregions: a conducting region R and a non-conducting region S. Let Γ denote the common portion of the boundaries of R and S and let n be the outward unit normal vector to the boundary surfaces. The magnetic vector potential A [Wb/m] and the electric scalar potential ϕ [V] are unknown functions. From Maxwell's equations, we can derive the following equations for the magnetic field in three-dimensional non-stationary eddy current problems; here,

ν is the magnetic reluctivity and σ is the conductivity.

$$\mathrm{rot}\left(\nu\,\mathrm{rot}\,A\right)+\sigma\frac{\partial A}{\partial t}+\sigma\,\mathrm{grad}\,\phi=J \ \text{ in } \Omega\times(0,\mathrm{T}), \tag{1a}$$

$$-\mathrm{div}\left(\sigma\frac{\partial A}{\partial t}+\sigma\,\mathrm{grad}\,\phi\right)=0 \ \text{in}\ R\times(0,\mathrm{T}), \tag{1b}$$

$$-\left(\sigma\frac{\partial A}{\partial t}+\sigma\,\mathrm{grad}\,\phi\right)\cdot n=0 \ \text{on}\ \Gamma\times(0,\mathrm{T}), \tag{1c}$$

$$A\times n=0 \ \text{on}\ \partial\Omega\times(0,\mathrm{T}), \tag{1d}$$

$$A\big|_{t=0}=A^0 \ \text{in}\ \Omega. \tag{1e}$$

The excitation current density $J\left[\mathrm{A/m^2}\right]$ satisfies the following continuity equation:

$$\mathrm{div}\,J=0 \ \text{ in } \Omega\times(0,\mathrm{T}). \tag{2}$$

2.2 The weak form and finite element approximation

Let $L^2(\Omega)$ be a space of functions defined in Ω and square summable in Ω with its inner product (. , .) and let $H^1(\Omega)$ be a space of functions in $L^2(\Omega)$ with derivatives up to the first order. We define V,U and W by

$$V\equiv\left\{v\in\left(L^2(\Omega)\right)^3;\mathrm{rot}\,v\in\left(L^2(\Omega)\right)^3,v\times n=0 \ \text{ on } \ \partial\Omega\right\},$$

$$U\equiv\left\{u\in H^1(R)\right\},$$

$$W\equiv\left\{w\in H^1(\Omega);w=0 \ \text{ on } \partial\Omega\right\}.$$

The weak form of equation (1) may be expressed as follows. Here A,ϕ are unknown functions $\left(\text{with}\,(A,\phi)\in V\times U\right)$ and A^*,ϕ^* are arbitrary test functions (again with

$(A^*, \phi^*) \in V \times U)$.

$$(\nu \operatorname{rot} A, \operatorname{rot} A^*) + \left(\sigma \frac{\partial A}{\partial t}, A^*\right) + (\sigma \operatorname{grad} \phi, A^*) = (J, A^*), \tag{3a}$$

$$(\sigma \operatorname{grad} \phi, \operatorname{grad} \phi^*) + \left(\sigma \frac{\partial A}{\partial t}, \operatorname{grad} \phi^*\right) = 0. \tag{3b}$$

We next divide the domain Ω into union of tetrahedra and discretize space. We approximate the magnetic vector potential using first-order Nedelec elements and we approximate the electric scalar potential and other quantities using the conventional first-order tetrahedral elements. Let V_h, U_h, W_h respectively denote the finite element spaces corresponding to V, U, W. Introducing the backward Euler method for time discretization (Δt : a time increment) allows us to write the finite element equation in the following form:

$$(\nu \operatorname{rot} A_h^{n+1}, \operatorname{rot} A_h^*) + \left(\frac{\sigma}{\Delta t} A_h^{n+1}, A_h^*\right) + (\sigma \operatorname{grad} \phi_h^{n+1}, A_h^*) = (\tilde{J}_h^{n+1}, A_h^*) + \left(\frac{\sigma}{\Delta t} A_h^n, A_h^*\right), \tag{4a}$$

$$\left(\frac{\sigma}{\Delta t} A_h^{n+1}, \operatorname{grad} \phi_h^*\right) + (\sigma \operatorname{grad} \phi_h^{n+1}, \operatorname{grad} \phi_h^*) = \left(\frac{\sigma}{\Delta t} A_h^n, \operatorname{grad} \phi_h^*\right). \tag{4b}$$

Here, for actual calculations, we use the conventional first-order tetrahedral element for $\tilde{J}_h^{n+1}$. For a correction obtained by considering Eq. (2), we approximate J^{n+1} and perform a pre-calculation as follows:

$$(\operatorname{grad} I_h^{n+1}, \operatorname{grad} I_h^*) = (J_h^{n+1}, \operatorname{grad} I_h^*). \tag{5}$$

After obtaining I_h^{n+1} by Eq. (5), we find the corrected approximate current density $\tilde{J}_h^{n+1}$ from the relation :

$$\tilde{J}_h^{n+1} = J_h^{n+1} - \operatorname{grad} I_h^{n+1}. \tag{6}$$

Note that $I_h^{n+1}, I_h^* \in W_h$.

2.3 Transient analysis considering the B–H characteristics

The magnetic reluctivity ν exhibits a material-dependent nonlinearity. In transient analysis, the values of ν are obtained at each time step from the *H–B* curve (Fig. 1)

obtained from measured data [5]. Denoting the magnetic reluctivity ν at the n-th time step by ν_h^{n} and substituting into Eq. (4a) yields

$$\left(\nu_h^{\mathrm{n}}\ \mathrm{rot}\ A_h^{\mathrm{n+1}}, \mathrm{rot}\ A_h^*\right)+\left(\frac{\sigma}{\Delta t}A_h^{\mathrm{n+1}}, A_h^*\right)+\left(\sigma\ \mathrm{grad}\,\phi_h^{\mathrm{n+1}}, A_h^*\right)=\left(\tilde{J}_h^{\mathrm{n+1}}, A_h^*\right)+\left(\frac{\sigma}{\Delta t}A_h^{\mathrm{n}}, A_h^*\right). \quad (7)$$

Thus, the value of the magnetic reluctivity ν_h^{n} obtained from the calculation for time step n is used in the computation for time step $\mathrm{n}+1$. We have

$$\begin{aligned}|H| &= \nu_i\left(|B|-|B_i|\right)+|H_i| \\ &= \nu_i|B|+\left(|H_i|-\nu_i|B_i|\right) \\ &= \left\{\nu_i+\frac{\left(|H_i|-\nu_i|B_i|\right)}{|B|}\right\}|B|,\end{aligned}$$

from which it follows that

$$\nu\left(|B|\right)=\nu_i+\frac{|H_i|-\nu_i|B_i|}{|B|}. \quad (8)$$

In these equations, $|B_i|\le|B|\le|B_{i+1}|$. If, in addition, $|B_0|\le|B|\le|B_1|$, then the following result holds:

$$\nu\left(|B|\right)=\nu_0\ . \quad (9)$$

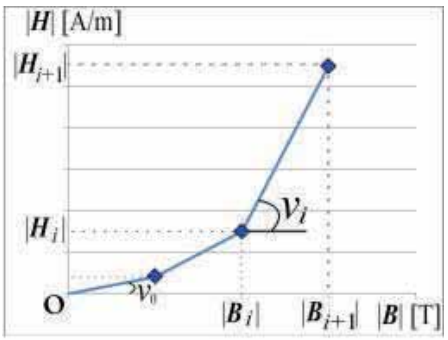

Fig.1. *H-B* curve

If we simply use the magnetic reluctivity at the time step for Eq. (8), it is not possible to obtain stable results. However, by introducing a weighting factor $w\left(0<w\le1\right)$, it is

possible to obtain stable values for the magnetic reluctivity [5]. The values of $\left|B_g^{\mathrm{n}}\right|$ at the centroids of the elements are obtained from the solution A_h^{n} at time step n and v_h^{n} is determined by the following relations:

$$v_{HB}^{\mathrm{n}} = v_i^{\mathrm{n}} + \frac{\left|H_i^{\mathrm{n}}\right| - v_i^{\mathrm{n}}\left|B_i^{\mathrm{n}}\right|}{\left|B_g^{\mathrm{n}}\right|},$$

$$v_h^{\mathrm{n}} = w\, v_{HB}^{\mathrm{n}} + (1-w) v_h^{\mathrm{n}-1}. \tag{10}$$

The value of v_h^{n} obtained from Eq. (10) is used in the computation for time step $\mathrm{n}+1$.

2.4 Transient analysis in the presence of rotation

If we work in a moving coordinate system fixed within a rotating body, then the basic equations (1) may still be valid. Thus, in the following treatment of rotating bodies, we consider Eq. (1) as holding within a moving coordinate system fixed within the rotating body and we subsequently transform this equation system back to a coordinate system fixed in space to apply Eq. (4) in the context of the finite element method. In this case, the time derivatives $\frac{\partial A}{\partial t}$ in Eq. (1) become Lagrange derivatives $\frac{DA}{Dt}$. On discretizing space into finite elements [6], we use the following approximate relation for the Lagrange derivative term at a point p in the rotating body at time $(\mathrm{n}+1)\Delta t$:

$$\frac{DA_h(x,(\mathrm{n}+1)\Delta t)}{Dt} \cong \frac{A_h(x,(\mathrm{n}+1)\Delta t) - A_h(x - v\Delta t, \mathrm{n}\Delta t)}{\Delta t}, \tag{11}$$

here, x denotes the coordinates of the point p and v is a given velocity vector (assumed to be constant here for simplicity). The quantity $A_h(x - v\Delta t, \mathrm{n}\Delta t)$ is known and $A_h(x,(\mathrm{n}+1)\Delta t)$ is the unknown quantity for which we wish to solve. Using superscripts n and $\mathrm{n}+1$ to denote time steps, the approximate values are written respectively as A_h^{n} and $A_h^{\mathrm{n}+1}$. Ultimately, the finite element equations simply recover Eqs. (4a) and (4b), but some ingenuity is needed to obtain A_h^{n}.

Thus, we now consider the determination of A_h^{n}. As shown in Fig. 2, due to the

rotation of the body, edge a–b is – at a time Δt s previously – at the position of edge a'–b'. As indicated in the figure, in most cases edge a'–b' is not defined at the edge of the finite element mesh. Consequently, we must use an interpolation scheme to estimate values of A_h^{n}. In accordance with the definition of the Nedelec element, we evaluate line integrals over all elements containing edge a'–b' as follows:

$$\begin{aligned} A_{\mathrm{a'-b'}}^{\mathrm{n}} l_{\mathrm{a'-b'}} &= \int_{\mathrm{a'}}^{\mathrm{b'}} A_h^{\mathrm{n}} \cdot s \,\mathrm{d}\, l \\ &= \int_{\mathrm{a'}}^{c'} A_h^{\mathrm{n}} \cdot s \,\mathrm{d}\, l + \int_{c'}^{d'} A_h^{\mathrm{n}} \cdot s \,\mathrm{d}\, l + \int_{d'}^{\mathrm{b'}} A_h^{\mathrm{n}} \cdot s \,\mathrm{d}\, l . \end{aligned} \tag{12}$$

Here, $A_{\mathrm{a'-b'}}^{\mathrm{n}}$ corresponds to the component of A_h^{n} on edge a'–b' and in the direction of that edge, $l_{\mathrm{a'–b'}}$ denotes the length of edge a'–b', and s denotes the unit tangent vector to each edge. By evaluating line integrals for each element in this way, we obtain a value for A_h^{n}.

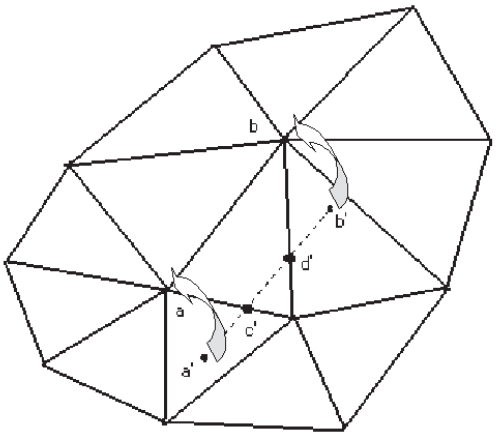

Fig. 2. Movement of an edge during Δt

3. Numerical Examples

3.1 Comparison with ADVENTURE_Magnetic for frequency response analysis

We confirm the validity of our procedure by comparing the results of a non-stationary eddy current analysis conducted using NEXST_Magnetic with the results of a frequency

response analysis conducted using ADVENTURE_Magnetic. By comparing with ADVENTURE_Magnetic, which has a proven track record for frequency response analysis, we can assess the accuracy of NEXST_Magnetic and obtain a thorough understanding of the real and imaginary parts of the frequency response analysis results obtained from ADVENTURE_Magnetic.

Frequency response analyses conducted using ADVENTURE_Magnetic return two types of results: real and imaginary parts. These agree with the results obtained using NEXST_Magnetic when the current density is maximum and 0, respectively.

Our computational model obtained eddy current analysis results for the infinite-length solenoidal coil in Fig. 3 [3]. The radius of the conductor was taken to be 0.1 m. The magnetic reluctivity v was taken to be $1/(4\pi)\times 10^7$ [m/H], while the conductivity σ of the conductor was taken to be 7.7×10^6 [S/m]. The frequency ω was $2\pi\times 60$ [rad/s]. The excitation current density J flowing through the coil was an AC current in the form $J_0 \cos \omega t$ [A/m^2] with $|J_0| = 50$ [A/m^2]. The NEXST_Magnetic analysis was conducted with all initial values A_h^0 set equal to 0 and Δt taken to be 1/(60×40). A total of 250 time steps were used, corresponding to 6.25 full cycles. The results of NEXST_Magnetic agree with the real parts of the ADVENTURE_Magnetic results at time steps 40, 80, 120, 160, 200, and 240 and they agree with the imaginary parts of the ADVENTURE_Magnetic results at time steps 50, 90, 130, 170, 210, 250. In this cake model, the magnetic flux density arises solely in the direction of the z axis, so we consider only the z component.

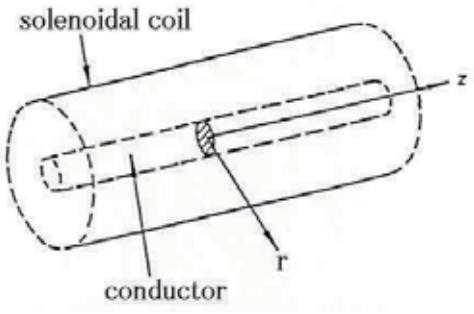

Fig.3. Solenoidal coil with unlimited length

Figure 4 compares the magnitude and direction of the magnetic flux density for points at which the excitation current density applied to the coil is a maximum (corresponding to the real part of the solution). To compute the relative error in each of these values, we compute the actual value using ADVENTURE_Magnetic and compare it with the results of NEXST_Magnetic.

Figure 4 shows the relative error for the magnetic flux density throughout the entire model. A relative error of between 1% and 2% is apparent at each time step.

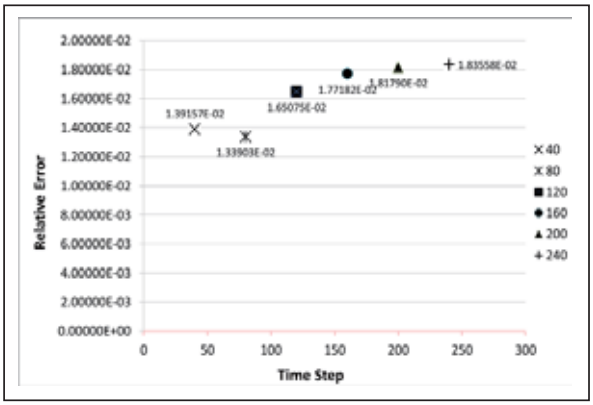

Fig.4. Magnetic flux densities in *z* direction
(Comparison of real part)

Figure 5 compares the magnitude and direction of the magnetic flux density for points at which the excitation current density applied to the coil is zero (corresponding to the imaginary part of the solution). As with the results shown in Fig. 4, there is a relative error of between 6% and 7% at each time step.

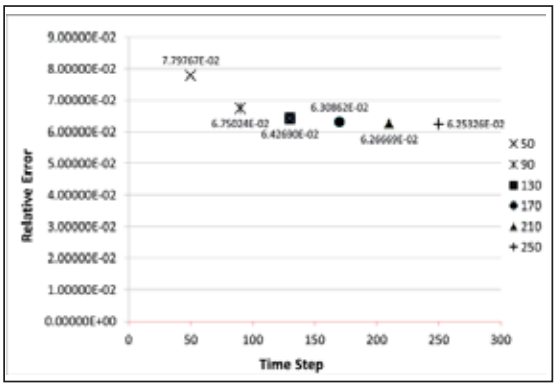

Fig. 5. Magnetic flux densities in *z* direction
(Comparison of imaginary part)

These results demonstrate that the results of transient analysis conducted using NEXST_Magnetic may be considered equivalent to the results of frequency response analysis.

3.2 A first analysis neglecting the B–H characteristics

As a numerical example, we consider the results of an eddy current analysis conducted for a rotating machine of the type shown in Fig. 6. This machine is composed of one fixed component and one rotating component and consists of 36 primary conductors and 44 secondary conductors. The model considered in this section does not account for the air gap between the fixed and rotating components. The magnetic reluctivity ν is $1/(4\pi)\times10^4\,[\mathrm{m/H}]$ for both the fixed and rotating components and $1/(4\pi)\times10^7\,[\mathrm{m/H}]$ for both the primary and secondary conductors. The conductivity σ of the conductor regions is $3.0\times10^7\,[\Omega/\mathrm{m}]$ and the frequency is $\omega=2\pi\times50[\mathrm{rad/s}]$. The excitation current density J flowing in the coil is an AC signal with the form $J_0\cos\omega t$ [A/m^2] where $|J_0|=6.61\times10^6$ [A/m^2]. It goes without saying that phase change of the excitation current density is suitably considered in our model.

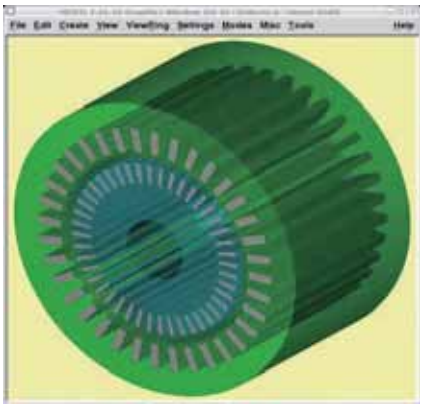

Fig. 6. A rotating machine

We considered computational models with 152,336 elements. The initial values A_h^0 were all set to zero. We chose a time step Δt equal to 1/(50×24) s and ran the computation for 72 time steps (three cycles as in Fig.7). The computation was executed on a desktop workstation having an Intel Core i7 920 CPU (2.66 GHz) and 24 GB of RAM.

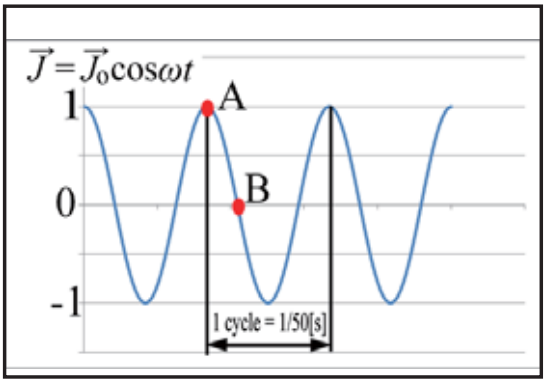

Fig. 7. Excitation current density

Figure 8 presents results for the magnetic flux density distribution on a cross-sectional slice through the center of the rotating machine at a time corresponding to point A in Fig. 7. Figure 9 presents similar results at a time corresponding to point B in Fig. 7. Comparison of these two plots reveals that the regions near the fixed primary conductor

in which the magnetic flux density is high are moving.

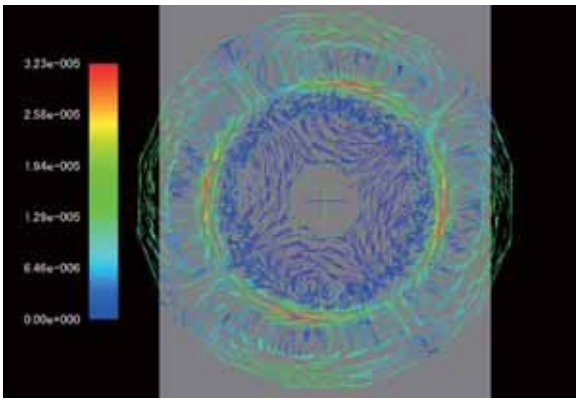

Fig. 8. Magnetic flux density for point A in Fig. 7

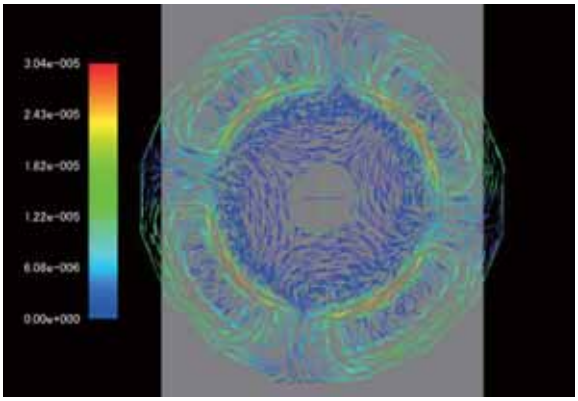

Fig. 9. Magnetic flux density for point B in Fig. 7

3.3 A second analysis accounting for the B–H characteristics

As in Section 3.2, we consider the results of an eddy current analysis conducted on a rotating machine. However, we now enhance our analysis by considering the *B–H* characteristics of the fixed and rotating components of the machine. Here, we use a weighting constant of value $w = 0.112$ and set the initial magnetic reluctivity v equal to the same values used in Section 3.2, namely, $1/(4\pi)\times 10^4\,[\mathrm{m/H}]$ for both the fixed and rotating components. The remaining analysis conditions are the same as those in Section 3.2.

In comparison with the computational results obtained without considering the *B–H* characteristics, Figs. 10 and 11 exhibit lower values in the magnetic flux density. In both figures, the maximum value becomes about 1/5. The color bars do not match those of Figs. 8 and 9.

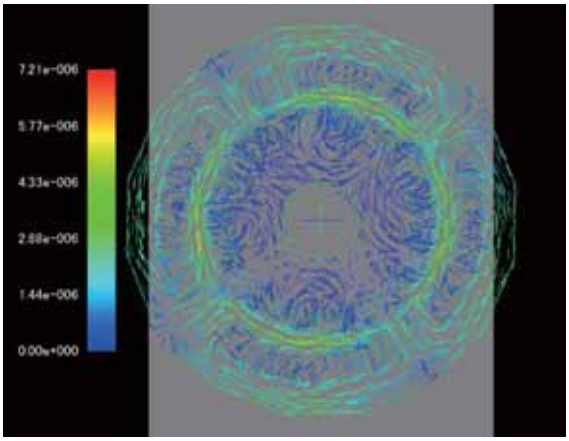

Fig. 10. Magnetic flux density for point A in Fig. 7

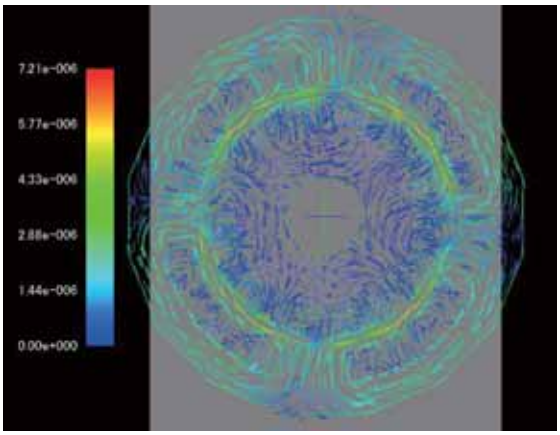

Fig. 11. Magnetic flux density for point B in Fig. 7

3.4 A computational model of a rotating machine with an air gap

The previous rotating machine model discussed in Section 3.2 does not account for the air gap. In addition, the shape of the coil is approximated as rectangular. We next consider a frequency response analysis (neglecting the *B–H* characteristics) conducted

using ADVENTURE_Magnetic on a new model, indicated in Fig. 12, based on the two points considered above.

Fig. 12. A rotating machine model with an air gap

We used the same computational conditions as in Section 3.2 and analyzed a model with 4,850,700 elements using a domain decomposition method. With a total of 80 parts, the computation time was approximately 12.25 h.

Figures 13 and 14 show the results. Comparison of these plots reveals that the regions of large magnetic flux density around the fixed primary conductor are moving, as in Section 3.2. It is also noted that there are regions with high magnetic flux densities near the air gap.

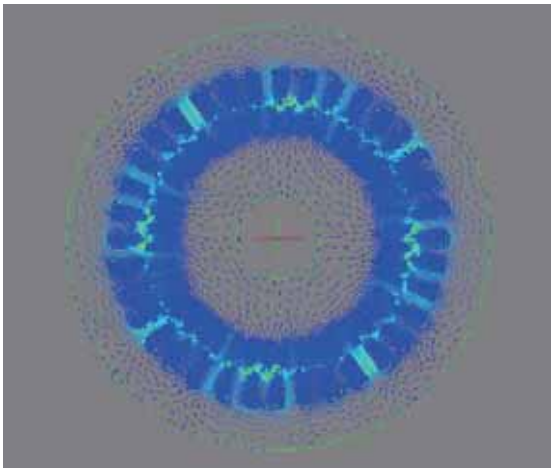

Fig. 13. Result of ADVENTURE_Magnetic (real part)

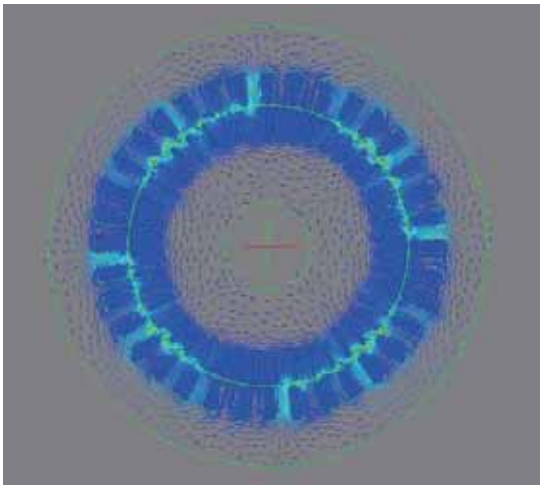

Fig. 14. Result of ADVENTURE_Magnetic
(imaginary part)

3.5 Consideration of rotation for a simplified rotating machine with an air gap

The previous rotating machine model discussed in Section 3.4 does not account for the movement of rotation. We finally consider a transient analysis considering the rotation (neglecting the *B–H* characteristics) conducted using NEXST_Magnetic on a simplified model, indicated in Fig. 15. The fixed component has 4 primary conductors and the rotating component also has 4 secondary conductors. The air gap is considered between

the fixed component and the rotating component. 20 kinds of meshes have been prepared for one cycle rotation and we are using different meshes for each time step.

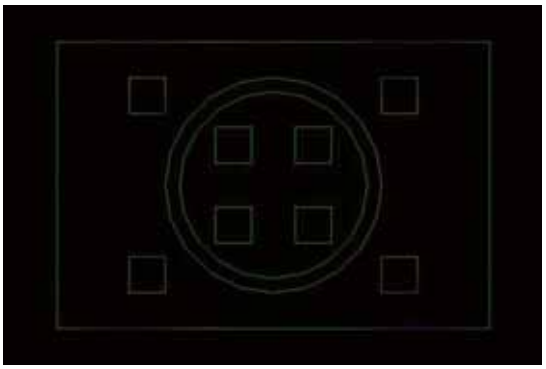

Fig. 15. A simplified rotating machine

Figure 16 shows the magnetic flux densities from the time step 1081 to 1084. As mentioned before, the previous position of the edge within the rotating component is searched for each time step. The conjugate gradient solver uses the previous step result for the initial value of each time step iteration.

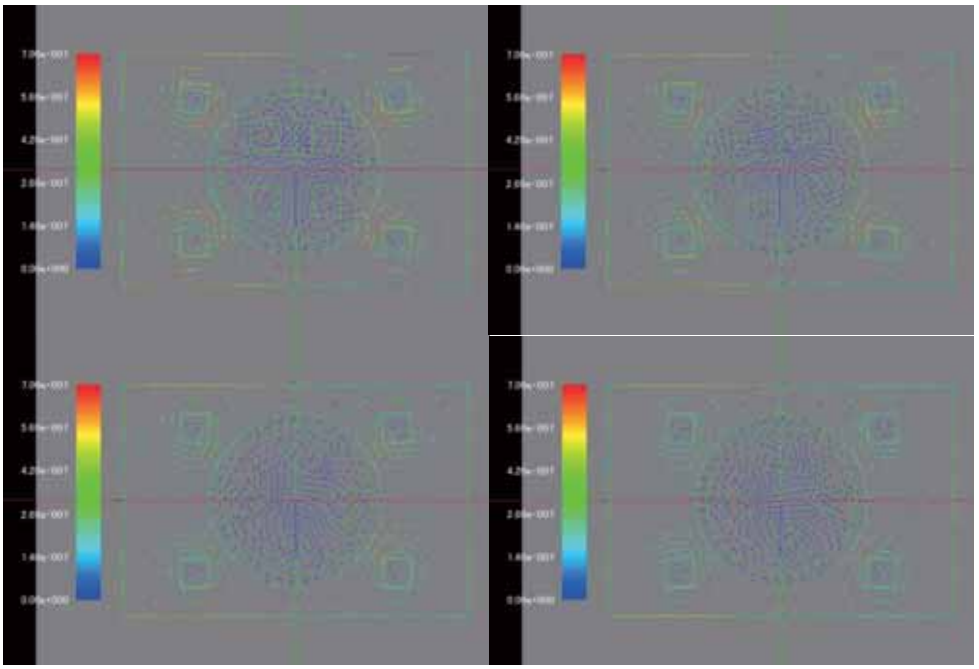

Fig. 16. The 4 step results of magnetic flux densities

4. Conclusions

We have used the $A-\phi$ method to analyze non-stationary eddy current problems. In near future, we plan to extend our computational models to larger-scale problems.

References

(1) Hiroshi Kanayama and Shin-ichiro Sugimoto : "Effectiveness of $A-\phi$ method in a parallel computing with an iterative domain decomposition method", IEEE TRANSACTIONS ON MAGNETICS, Vol.42, No.4, pp.539-542 (2006)

(2) ADVENTURE Project home page "http://adventure.sys.t.u-tokyo.ac.jp/jp/"

(3) Hiroshi Kanayama, Daisuke Tagami and Shin-ichiro Sugimoto : "A finite element computation of unsteady eddy current problems using the $A-\phi$ method", Proceedings of the 8th JSCES Conference, Vol.8, pp.687-690 (2003) in Japanese

(4) NEXST_Magnetic, Version 1.0 (2005) "http://www.ciss.iis.u-tokyo.ac.jp/fsis/index.html"

(5) Hiroshi Kanayama, Ryuji Shioya, Daisuke Tagami and Hongjie Zheng : "A numerical procedure for 3-D nonlinear magnetostatic problems using the magnetic vector potential", THEORETICAL AND APPLIED MECHANICS, Vol.50, pp.411-418 (2001)

(6) Shin-ichiro Sugimoto and Hiroshi Kanayama: "Eddy current computation with moving conductors", IEEJ SA-05-9, RM-05-9, pp.47-50 (2003) in Japanese